

# Glass transition in fullerenes: mode-coupling theory predictions

M. J. Greenall and Th. Voigtmann  
*SUPA, The University of Edinburgh, School of Physics,  
JCMB The King's Buildings, Edinburgh EH9 3JZ, U.K.*  
(Dated: March 23, 2022)

We report idealized mode-coupling theory results for the glass transition of ensembles of model fullerenes interacting via phenomenological two-body potentials. Transition lines are found for  $C_{60}$ ,  $C_{70}$  and  $C_{96}$  in the temperature–density plane. We argue that the observed glass-transition behavior is indicative of kinetic arrest that is strongly driven by the inter-particle attraction in addition to excluded-volume repulsion. In this respect, these systems differ from most standard glass-forming liquids. They feature arrest that occurs at lower densities and that is stronger than would be expected for repulsion-dominated hard-sphere-like or Lennard-Jones-like systems. The influence of attraction increases with increasing the number of carbon atoms per molecule. However, unrealistically large fullerenes would be needed to yield behavior reminiscent of recently investigated model colloids with strong short-ranged attraction (glass-glass transitions and logarithmic decay of time-correlation functions).

PACS numbers: 61.48.+c, 64.70.Pf

## I. INTRODUCTION

Fullerenes, hollow cages of carbon atoms ( $C_N$ ), were discovered and first synthesized in the mid-nineteen-eighties [1, 2]. The behaviour of  $C_{60}$  has been particularly thoroughly studied. There are many reasons for the interest in these molecules, notably their stability and near-spherical structure as single molecules.

Liquids composed of fullerene molecules have long been proposed, but there are two main fundamental issues concerned with their existence. Molecular dynamics simulations (Refs. [3, 4, 5, 6, 7]) predict that individual fullerene molecules should remain intact up to temperatures of several thousand K, and arc discharge experiments indicate that they are stable on at least the 0.1 ms timescale. However, when fullerenes are heated in bulk to relatively low temperatures (around 1200 K), a dissociation into forms of amorphous carbon sets in (e.g. Refs. [8, 9, 10, 11]). This instability could be due to impurities [12], or be a collective effect involving inter-fullerene interactions [9].

Secondly, even if the stability of the high-temperature bulk fullerene system is assumed, there has been considerable disagreement on the characteristics of its equilibrium phase diagram, in particular the existence or absence of a thermodynamically stable liquid phase [13, 14].  $C_{60}$  appears to be a borderline case [15, 16], and the gas–liquid spinodal eventually shifts into the metastable region below the fluid–crystal transition with increasing number of carbon atoms per molecule,  $N$  [17, 18]. For this reason, model fullerenes have been mentioned as analogues of short-range attractive systems [19, 20]. Such systems can be realized in colloidal suspensions where added free polymer induces an effective interaction whose width and strength can be fine-tuned. They are frequently modeled by a square-well system (SWS), i.e., a hard-sphere (HS) potential supplemented by a square-well attraction of finite range. As this range is decreased,

the gas–liquid critical temperature drops, until it eventually falls into the fluid–crystal coexistence region. Thus the metastability of the liquid phase can be taken as a signature of ‘short-ranged’ attractions (see Refs. [21, 22]). Indeed, common models for fullerene interaction assume LJ-like interactions between the individual carbon atoms, which are of short range compared to the large diameter of the  $C_N$  molecule itself. Furthermore, at high enough temperatures, the internal degrees of freedom of the fullerene molecules should not play a major role, since each molecule is able to rotate freely [23]. In this way, fullerenes suggest themselves as a molecular system that might display the hitherto purely colloidal class of phenomena associated with short-ranged interparticle attraction.

If one is concerned with the kinetic phenomena of the (perhaps metastable) fluid, this analogy raises an interesting question. In experiments on colloid-polymer mixtures [24, 25] and theoretical studies on the SWS or similar models [26, 27], qualitatively new dynamical features are connected to the short range of the attractions. In particular, these systems form glasses; that is, amorphously arrested states, whose nature changes as the importance of interparticle attraction over the core repulsion changes. At very high temperatures, the glasses formed from dense fluids are driven almost exclusively by the core repulsion – as particles become trapped in *cages* of their neighbors – and are hence qualitatively similar to hard-sphere glasses. Addition of attractive interactions that are comparable to or bigger in range than the typical interparticle separation in this high-density fluid has a small effect on the kinetics, since these add up to a more or less flat background [28]. In particular, the glass transition in the Lennard-Jones (LJ) model (after all a good representation of many molecular liquids) is, according to recent theoretical studies [29], *repulsion-driven* over the entire temperature range. The localization length of the particles in such glasses is comparable to 10% of the core

diameter, in agreement with the Lindemann criterion for freezing, and little influenced by the range of the inter-particle attraction. However, if sufficiently short-ranged and strong attractions are present, a qualitatively different glass is found when the thermal energy becomes comparable to or lower than the attraction depth, as *bonding* provides a second particle-trapping mechanism. Consequently, the range over which particles are localized in such an *attraction-driven* glass scales with the range of this attraction and can be an order of magnitude smaller than the one predicted for repulsive glass. Furthermore, their degree of arrest is much larger; in particular they appear mechanically much stiffer than comparable standard glasses. The intriguing question then posed by this analogy is: do fullerenes, under certain conditions, form attractive glasses, or at least ones that display some characteristics of the colloidal attractive glasses?

In this paper, we explore theoretically the above analogy on the kinetic level between the liquid of model fullerenes and short-range-attractive model colloids. Recent molecular-dynamics (MD) simulations on model fullerene liquids [30, 31, 32] have shown that there occurs a positional glass transition in model fullerene liquids at high density, connected with a freezing-in of the molecules' translational degrees of freedom, and not to be confused with the rotational glass transition occurring in fullerene crystals below room temperature [33]. From the MD data, it was concluded that the positional glass transition is essentially a repulsion-dominated glass transition reminiscent of hard spheres. However, this judgement was based solely on the shape of the transition line  $\rho_g(T)$ . Our study shall provide a theoretical basis for the investigation of such fullerene glasses, by applying the mode-coupling theory of the glass transition (MCT) [34] to the model potentials for fullerenes employed in these and similar MD simulations. MCT has been very successful in describing the details of the repulsive-to-attractive crossover in the SWS [26, 27], and hence should be well suited to investigate the analogous question here. It will allow us to predict not only the qualitative shape of the glass transition line, but also the strength of the arrest and the form of the time decay of density fluctuations near to the transition. The investigation of kinetic effects might also be interesting for a further understanding of the destabilization of fullerenes (as far as kinetic cooperative effects are involved).

We start by giving a brief introduction to the fullerene models used in this study (Sec. II), and a sketch of MCT and the calculation of glass-transition lines in the density-temperature diagram of various fullerenes (Sec. III). Section IV presents our main results, after which a discussion follows in Sec. V.

## II. FULLERENE MODELS

For temperatures high enough so that internal modes of the  $C_N$  molecules become unimportant, one can model

the fullerene bulk system by particles interacting with a spherically symmetric pair potential. A popular model of this kind is due to Girifalco [35]. This potential can be applied to fullerenes formed from any number  $N$  of carbon atoms; however, the assumption of spherical shape and the neglect of intramolecular vibrations become more and more questionable the larger the molecules. The model assumes Lennard-Jones interactions with experimentally determined parameters between the individual carbon atoms, which are then integrated over hollow spheres representing the buckyball molecules. This yields

$$V(r) = -\alpha \left[ \frac{1}{s(s-1)^3} + \frac{1}{s(s+1)^3} - \frac{2}{s^4} \right] + \beta \left[ \frac{1}{s(s-1)^9} + \frac{1}{s(s+1)^9} - \frac{2}{s^{10}} \right], \quad (1)$$

where  $r$  is the centre-centre separation of two fullerene molecules of diameter  $d$ , and  $s = r/d$ . The constants  $\alpha$  and  $\beta$ , tabulated in Ref. [35], are proportional to  $N^2$ . A suitable radius  $d(N)$  can be inferred from experiment and simulation [35, 36, 37, 38], or from the assumption  $d \propto \sqrt{N}$  [39, 40]. We will use the Girifalco potential in our work for  $N = 60, 70$ , and  $96$ , the most common low- $N$  fullerenes.

Data from *ab initio* calculations on  $C_{60}$  can be better fitted by a potential due to Pacheco and Ramalho (PR) [41]. One combines a long-range van der Waals expression with a short-ranged Morse-potential term,

$$V_{\text{PR}}(r) = F(r) \times M(r) + [1 - F(r)] \times W(r), \quad (2a)$$

$$W(r) = -C_6/r^6 - C_8/r^8 - C_{10}/r^{10} - C_{12}/r^{12}, \quad (2b)$$

$$M(r) = M_0 \exp[\tau(1 - r/d_0)] ((\tau(1 - r/d_0) - 2)), \quad (2c)$$

where  $F(r)$  describes the cross-over between the two,

$$F(r) = (1 + \exp[(r - \mu)/\delta])^{-1}. \quad (2d)$$

$C_6$  and  $C_8$  may be determined from density functional theory, whilst  $C_{10}$ ,  $C_{12}$ ,  $M_0$ ,  $d_0$ ,  $\tau$ ,  $\mu$ , and  $\delta$  are fitting parameters tabulated in Ref. [41]. The PR potential is somewhat softer than the Girifalco potential and appears superior in a number of predictions, but its application to larger fullerene molecules is not straightforward. For our discussion of qualitative features, the PR potential serves to demonstrate to what extent our results depend on the precise form of the potential chosen.

In comparing results for different-sized fullerenes, we need to introduce suitable natural scales of energy and length. An obvious choice for the energy scale is  $T^* = k_B T/\epsilon$ , where  $\epsilon$  is the magnitude of the potential at its minimum. A convenient choice for the unit of length is given by the Barker-Henderson effective diameter [42], letting  $r^* = r/\sigma_{\text{eff}}$  with

$$\sigma_{\text{eff}} = \int dr [1 - \exp(-V_{\text{rep}}(r)/(k_B T))]. \quad (3)$$

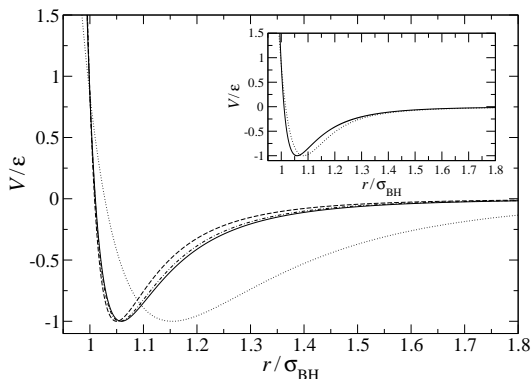


FIG. 1: Girifalco potentials for  $C_{60}$ ,  $C_{70}$ , and  $C_{96}$  (solid, dash-dotted, and dashed lines), in units of reduced temperature and the Barker-Henderson effective diameter  $\sigma_{\text{eff}}$ . The Lennard-Jones potential is shown as a dotted line. Inset: comparison of the Girifalco (solid line) and the Pacheco-Ramalho (dotted) potentials for  $C_{60}$ .

$V_{\text{rep}}$  is the repulsive part of the potential only,  $V_{\text{rep}} = V(r)$  for  $r \leq r_0$ , and zero otherwise, where  $r_0$  is the point for which  $V(r_0) = 0$ . As  $T \rightarrow \infty$ , we recover from this  $\sigma_{\text{eff}} \rightarrow \sigma$ , i.e. the hard-core diameter of the Girifalco potential, and, for hard-sphere systems,  $\sigma_{\text{eff}} \equiv \sigma$ . Note however, that the approach to the hard-core limit is extremely slow: for  $C_{60}$ ,  $\sigma_{\text{eff}} \approx 1.821\sigma$  at the highest temperatures considered ( $T = 50000$  K). For later comparison we also note that a purely repulsive potential that incorporates all soft-core effects of the Girifalco potential may be constructed following the Weeks-Chandler-Andersen (WCA) prescription [43],

$$V_{\text{cut}}(r) = \begin{cases} V(r) + \epsilon & r \leq r_- \\ 0 & r > r_- \end{cases} \quad (4)$$

Here,  $r_-$  is the position of the potential minimum. Abramo *et al.* [30, 31, 32] use this potential to define  $\sigma_{\text{eff}}$  according to Eq. (3). We refer to this as the WCA- $\sigma_{\text{eff}}$  in the following. If one is interested in discussing changes in the effective range of the potential with changing  $N$ , this definition appears disadvantageous, since it includes part of the change of  $r_-/r_0$  in the definition of  $\sigma_{\text{eff}}$ . The approach of this effective diameter to the hard-sphere limit  $\sigma$  is even slower than that of the Barker-Henderson definition: for  $C_{60}$ ,  $\sigma_{\text{BH}} \approx 1.827\sigma$  at  $T = 50000$  K. The advantage of  $V_{\text{cut}}$  lies in the fact that it includes the entire section of the potential where  $\partial_r V(r) > 0$ , and a comparison of MCT results based on  $V_{\text{cut}}(r)$  and the full  $V(r)$  will be used in the following to separate out those dynamical effects arising from attractive forces.

The Girifalco potentials for  $C_{60}$ ,  $C_{70}$ , and  $C_{96}$ , are shown in Fig. 1 in units of reduced temperature and the Barker-Henderson  $\sigma_{\text{eff}}$ . They show a weak dependence of the minimum position on  $N$ ,  $r_-^* \sim 1/(\text{const.} + \sqrt{N})$ :  $C_{96}$  might therefore be expected to display more evidence of attraction-driven glassy behavior than  $C_{60}$ . Even for  $N = 60$ , the minimum is significantly more short-ranged

than in the LJ potential representative for standard liquids, shown as a dotted line for comparison. Also shown (in the inset) is the PR  $C_{60}$  potential. The softness of the repulsive component of the PR interaction means that its Barker-Henderson diameter is smaller than that of the Girifalco  $C_{60}$  system, and the potential is shifted to higher  $r/\sigma_{\text{BF}}$ .

To apply MCT to any of the above potentials, one requires the equilibrium static structure factor,  $S(q)$ , corresponding to  $V(r)$ . The liquid-state theory to approximate  $S(q)$  is unconnected to MCT. For the Girifalco potential, we solve the Ornstein-Zernike (OZ) equation numerically to determine the direct correlation function  $c(q)$  (and with it  $S(q) = 1/(1 - \rho c(q))$ ), using the hypernetted-chain (HNC) and Percus-Yevick (PY) closure approximations [44]. These both have a known problem termed thermodynamic inconsistency: two equivalent routes to calculate the equation of state from them give different results. Much effort has been devoted to improving upon this deficiency. However, for an application of MCT, this issue is usually unimportant. As we shall explain below, the MCT integrals are not sensitive to the  $q \rightarrow 0$  region of  $c(q)$ , perhaps with the exception of a narrow region directly surrounding the spinodal of the model. Instead, they rely on a reasonable description of the  $q \gtrsim q_{\text{peak}}$  region, where  $q_{\text{peak}}$  is the first sharp diffraction peak. Similarly, the precise position of the equilibrium phase-transition lines, and even whether the approximation predicts a stable or only meta-stable liquid, is not important here, other than by typically setting an overall shift in the temperature scale. We have chosen HNC and PY to indicate boundaries between which many more refined closure schemes will vary our results [45]. In particular, most of our discussion is based around the PY approximation, since we found it to give more reasonable results when probing the hard-core part of the potential at very high temperatures. The numerical algorithm we employ to calculate  $S(q)$  is due to Labík *et al.* [46]; we used a wave-vector grid of 4096 points with a cutoff  $Q = 367.6 \text{ nm}^{-1}$  ( $R = 35 \text{ nm}$  for the radial distribution function  $g(r)$ ). Our calculated  $S(q)$  (using both PY and HNC closures) for  $T = 1900 \text{ K}$ ,  $\rho = 0.74 \text{ nm}^{-3}$  compares well (outside the  $q \rightarrow 0$  region discussed above) with molecular dynamics data for the corresponding state point published by Alemany *et al.* in Ref. [47].

### III. MODE-COUPLING THEORY OF THE GLASS TRANSITION

Let us present a brief outline of the (idealized) MCT description of structural glass transitions. For in-depth reviews, the reader is referred to Refs. [34, 48, 49].

MCT aims to describe the dynamical arrest that happens in dense liquids: even in the absence of a thermodynamic phase transition, the viscosity and, more generally, the relaxation times for many time-dependent fluctuations in the system increase sharply. As the glass tran-

sition is reached, the fluctuations are no longer able to decay to zero (as it is the case in a liquid), but a certain amount remains “frozen” in the still amorphous system. The theory describes this as a feedback mechanism driven by slow density fluctuations.

The most convincing evidence for the MCT scenario has come from colloidal systems, although the theory deals with both colloidal and molecular liquids alike. In the latter, however, the MCT transition is “avoided” due to additional relaxation paths called hopping processes and not captured in the theory. The MCT transition line  $T_c(\rho)$ , or equivalently  $\rho_c(T)$ , can still be inferred from experimental data by means of scaling laws the theory provides for the dynamics close to its idealized transition. However, due to the presence of hopping, the calorimetric glass transition  $T_g$  will be lower, so that  $T_g < T_c$  or equivalently  $\rho_g > \rho_c$ . The MCT transition point still indicates a change in transport mechanism from liquid-like to solid-like, although not a complete arrest. In this paper, we are concerned not with a precise determination of the MCT transition point, but rather with its qualitative changes upon varying control parameters such as temperature  $T$  or density  $\rho$ , and with the spatial structure of the resulting amorphous solid. These features of the glass are usually captured quite well by MCT [48].

The structure of the glass shall be characterized by its Debye-Waller factor (also called form factor or non-ergodicity parameter, NEP),  $f^c(q)$ : it quantifies the degree of arrest of density fluctuations at a wave vector  $\mathbf{q}$  in the glass. It is given by  $f^c(q) = \lim_{t \rightarrow \infty} \phi^c(q, t)$ , the long-time limit of the normalized density autocorrelation function,  $\phi(q, t) = \langle \varrho(\mathbf{q}, t)^* \varrho(\mathbf{q}, 0) \rangle / \langle |\varrho(\mathbf{q}, 0)|^2 \rangle$ , at the transition. Here,  $\varrho(\mathbf{q}, t) = \sum_{k=1}^N \exp[i\mathbf{q} \cdot \mathbf{r}_k(t)]$  are the (Fourier-transformed) density fluctuations,  $\mathbf{r}_k(t)$  are the individual particle positions, and  $\langle \cdot \rangle$  denotes a canonical average.  $\langle |\varrho(\mathbf{q}, 0)|^2 \rangle = S(q)$  is the static structure factor of the system. Even on the liquid side of the glass transition and in presence of hopping processes,  $f^c(q)$  can be determined from the time-dependent density correlation function.  $\phi(q, t)$  (as a function of  $\log t$ ) close to  $T_c$  develops a two-step process consisting of a “fast” decay towards its “plateau value”  $f^c(q)$ , followed by a slow final decay to zero. The time window over which  $\phi(q, t)$  stays close to its plateau extends as  $T_c$  is reached, and similar plateaus occur in many dynamical quantities. The mean-squared displacement (MSD) of a tracer particle for example exhibits a plateau that is directly connected to the localization length  $r_s$  of this tracer. Also the width of the  $f^c(q)$ -versus- $q$  curve gives an indication of the inverse localization length in the glass, since it closely follows the plateau value for the tagged-particle density correlator,  $f^{s,c}(q) \approx \exp[-q^2 r_s^2]$ , where the latter approximation holds for small  $q$ . Attractive glasses are characterized by a significantly reduced localization length, and consequently exhibit  $f^c(q)$ -versus- $q$  curves that follow a much broader envelope than that found in standard hard-sphere or LJ glasses.

Within MCT, the equation determining  $f^c(q)$  reads

$$\frac{f(q)}{1 - f(q)} = m[f](q), \quad (5)$$

to be evaluated at the transition point.  $m$  is the MCT memory kernel,

$$m[f] = \frac{\rho}{2q^2} \int \frac{d^3k}{(2\pi)^3} V(\mathbf{q}, \mathbf{k}) f(k) f(p), \quad (6a)$$

with  $\mathbf{p} = \mathbf{q} - \mathbf{k}$ . The  $V(\mathbf{q}, \mathbf{k})$  constitute the coupling constants of the theory, and they are determined completely in terms of the equilibrium static structure of the system; more precisely in terms of the direct and the triplet correlation function. Lacking a reasonable expression for the latter, one usually drops it (approximating three-point averages by a convolution approximation; this is not connected to the neglect of three-body terms in the potential). One then gets

$$V(\mathbf{q}, \mathbf{k}) = S(q)S(k)S(p) \left[ \frac{\mathbf{q} \cdot \mathbf{k}}{q} c(k) + \frac{\mathbf{q} \cdot \mathbf{p}}{q} c(p) \right]^2. \quad (6b)$$

In this sense,  $S(q)$  is the sole input to MCT. In particular, temperature effects enter only through their effect on  $S(q)$ . The  $k$ -integration in Eq. (6a) is responsible for suppressing finite variations in the form of  $c(q \rightarrow 0)$ , i.e., the influence of thermodynamic effects.

Eq. (5) in general has many solutions  $\tilde{f}(q)$ ; the NEP  $f(q)$  is the largest positive, real of these. As the control parameters and thus the coupling constants  $V$  are varied smoothly, bifurcations in Eq. (5) can occur, leading to a (generally) non-smooth jump for  $f(q) = 0$  to  $f(q) > 0$ . These bifurcations are the MCT glass transitions. They are found by a bisection search in  $\rho$  (at any given fixed  $T$ ), repeatedly solving Eq. (5) numerically until the transition point  $\rho_c(T)$  is located with the desired accuracy. To this end, wave vectors are discretized to a grid of  $M$  points with spacing  $\Delta q$ . The results presented below are typically obtained for  $M = 315$  and  $\Delta q = 0.4$ , with values as large as  $M = 600$  ( $\Delta q = 0.04$ ) for the SWS.  $S(q)$  was obtained as explained above, on a grid with spacing  $\Delta \rho = 0.01 \text{ nm}^{-3}$  for each temperature and interpolated linearly between those points; since  $S(q)$  varies smoothly, this interpolation leads to negligible errors. The results were checked for representative points with finer  $q$  ( $\Delta q = 0.2$ ) and  $\rho$  ( $\Delta \rho = 0.001 \text{ nm}^{-3}$ ) grids, and with larger ranges ( $M = 420$ ).

Each point on the MCT transition line is characterized by a real number  $1/2 \leq \lambda \leq 1$ , called the exponent parameter, that can be calculated knowing the coupling constants and  $f^c(q)$ . For the standard glass transition there holds  $\lambda < 1$ , and the decay of the density correlation function in the liquid is, asymptotically close to the transition, governed by two power laws:  $\phi(q, t) - f^c(q) \sim t^{-a}$  for the relaxation towards the plateau, and  $\phi(q, t) - f^c(q) \sim -t^b$  for the initial decay

from this plateau. The exponents  $a$  and  $b$  are determined by  $\lambda$ ,

$$\frac{\Gamma(1-a)^2}{\Gamma(1-2a)} = \lambda = \frac{\Gamma(1+b)^2}{\Gamma(1+2b)}. \quad (7)$$

The case  $\lambda \rightarrow 1$  (corresponding to  $a \rightarrow 0$  and  $b \rightarrow 0$ ) signals the breakdown of this power-law asymptotic expansion for  $\phi(q, t)$ , and points with  $\lambda = 1$  are termed higher-order glass transitions. In their vicinity, the asymptotic shape of correlation functions is better described by powers of  $\log t$  [50]. Such higher-order singularities have been found in the short-range attractive colloidal systems discussed above. There, they indicate a discontinuous cross-over between two qualitatively distinct types of glass – the one driven by repulsive caging, and the one driven by attractive bonding. The higher-order transition point vanishes for larger attraction ranges,  $\delta > \delta_c$ , with  $\delta_c \approx 0.045$  in the SWS. But even for  $\delta$  larger than but close to  $\delta_c$ , there remains a region along the glass-transition line  $T_c(\rho)$  where  $\lambda$  attains a maximum close to unity and where precursors of the higher-order transition have been found experimentally or in simulations [24, 25, 51, 52]. Hence the approach of  $\lambda$  to unity upon lowering the temperature in a system with attractive interactions can be taken as indicative for the crossover to an attraction-driven glass.

#### IV. RESULTS

Let us start by discussing the MCT results for the (idealized) glass-transition lines in the temperature–density plane,  $T_c(\rho)$ . Fig. 2 shows the transition lines for  $C_{60}$ ,  $C_{70}$ , and  $C_{96}$ . Results are shown using both the HNC (filled squares) and the PY (filled circles) closures to the OZ equation, in order to indicate the degree of uncertainty imposed on the MCT results by different approximations to  $S(q)$ . The respective no-solution boundaries for the two closures are also shown (HNC: open squares; PY: open circles); they can be taken as a rough approximation to the gas–liquid spinodal. Note that the binodal, as well as the freezing and melting lines, being thermodynamic rather than kinetic in origin, are not shown.

There is a small but noticeable difference between the glass transition curves calculated within the two different closure approximations. Since HNC and PY can be seen as limiting cases for a number of more refined closure schemes [45], we take the difference between the two transition lines to be an indication of that error contribution to  $T_c(\rho)$  that is not inherent to MCT. Note that even if the difference is small in terms of the critical density  $\rho_c$ , it can still lead to a significant uncertainty in determining  $T_c$ , as the lines run nearly vertically in the  $T$ -versus- $\rho$  plots shown. The PY-MCT transition is consistently shifted towards lower coupling strength (smaller  $\rho$  and higher  $T$ ) compared to the HNC-MCT line. This is different from the estimated spinodal regions, where

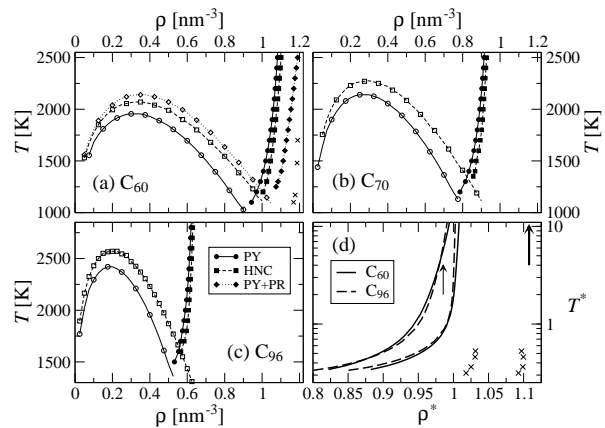


FIG. 2: MCT-glass transition lines (filled symbols and lines in panel d) for  $C_{60}$ ,  $C_{70}$ , and  $C_{96}$  models: in panels (a) to (c), solid (dashed) lines with circle (square) symbols are the results for the Girifalco potential using the PY (HNC) closure for  $S(q)$ . Diamond symbols with dotted lines correspond to the PR potential for  $C_{60}$ . Lines with open symbols indicate the loci of points below which no solution for  $S(q)$  exists within the OZ closure (indication of the gas–liquid spinodal). Crosses are MD simulation results from Ref. [30]. Panel (d) shows the PY and MD (Ref. [30]) results in terms of dimensionless quantities  $\rho^*$  and  $T^*$  defined according to the BH (left) and WCA (right) prescriptions (see text for details). The thin (thick) arrows in panel (d) indicate the  $T \rightarrow \infty$  transition point for hard spheres as calculated from MCT (determined from experiment),  $(6/\pi)\rho^* = 0.516$  (0.58)

PY generally estimates lower  $T$  than HNC. This underlines that different aspects of the equilibrium structure are responsible for the two phenomena.

Fig. 2 also exhibits results for  $C_{60}$  based on the PR potential together with the HNC closure approximation [diamonds and dotted lines in panel (a)]. This considerably softer potential displaces the MCT glass-transition line to even higher densities. The uncertainty coming from the potential modeling is much greater than the one due to different OZ closures. Also included in the figure as crosses are some MD simulation results [30] for  $\rho_g(T)$ , determined from the nonequilibrium system following a temperature-quench. As expected (due to the cutting off of the MCT glass transition by hopping processes),  $\rho_g > \rho_c$ . But the shape of the two lines is roughly similar.

The fullerene diameter and energy scale both change upon varying  $N$ , leading to a known shift of the phase diagram towards lower  $\rho$  and higher  $T$  [17, 18]; the MCT transition line follows this trend as expected. Panel (d) of Fig. 2 is an attempt to scale out these broad effects: it shows the transition lines in reduced units as discussed above, using both the BH and WCA definitions of the effective diameter  $\sigma_{\text{eff}}$ . Results for  $C_{70}$  are omitted to avoid overcrowding. The difference between the two rescalings is marked – use of the WCA- $\sigma_{\text{eff}}$  shifts the glass transition line to higher  $\rho^*$  for all  $T^*$ . This can be understood by recalling that the WCA definition includes a section

of repulsive potential ( $V(r) < 0$ ,  $\partial_r V(r) > 0$ ) omitted in the BH approach, leading to a higher  $\sigma_{\text{eff}}$ . However, the two representations of our results have two major features in common. Firstly, both show a clear bending across of the glass transition lines to lower  $\rho^*$  at lower  $T^*$ , even after scaling out (through  $\sigma_{\text{eff}}$ ) of the growth in the effective size of the repulsive core as the temperature is decreased. Secondly, the transition lines for  $C_{96}$  are at markedly lower  $\rho^*$  than those for  $C_{60}$  at lower  $T^*$ , even though the different fullerene lines are close (and cross if BH- $\sigma_{\text{eff}}$  is used) at high  $T^*$ . Both these points are suggestive of the enhancement of arrest through (relatively) short-ranged attraction in these systems.

However, the form of the glass transition lines at high  $T^*$  suggests that we might encounter problems in using these rescaled plots to make firm conclusions about the nature of the glassy behavior. As  $T^* \rightarrow \infty$ , one expects the potential to become more and more HS-like (since the Girifalco potential has a hard-core excluded volume contribution), and hence the transition line to approach the HS value,  $\rho_c^* = 0.516(6/\pi)$  [53] for the MCT-PY calculation. Similarly, the simulation values for  $\rho_g^*$  are expected to approach the experimentally-determined value for the HS glass transition,  $\rho_g^* \approx 0.58(6/\pi)$ . Both asymptotic values are indicated in panel (d) of Fig. 2 as vertical arrows. An ideal choice of effective diameter would collapse the glass transition lines to the HS  $\rho_c^*$  (making them vertical) as soon as the temperature became large compares to the potential depth. However, both the definitions used here fail to produce any collapse of our MCT results over the temperature ranges considered here, despite the fact that our highest  $T^*$  correspond to  $T \approx 50000$  K. In addition, both rescalings move the glass transition lines at high  $T^*$  to higher  $\rho^*$  than the HS value – a result of the slow approach of these  $\sigma_{\text{eff}}$  to the HS diameter  $\sigma$  referred to in Section II.

Note that in Refs. [30, 31], using the WCA- $\sigma_{\text{eff}}$ , it was concluded that  $\rho_g^* \approx 0.574(6/\pi)$  is essentially equal to the hard-sphere transition value and independent of  $T^*$ , and hence that the glass formation was entirely repulsion-driven. However, given the lack of a clear-cut physical reason for choosing a particular  $\sigma_{\text{eff}}$ , one needs to be careful in drawing conclusions solely from the numerical values of  $\rho_g^*$  defined in terms of such a  $\sigma_{\text{eff}}$  over a limited temperature range. In the following, we will try to find signatures of attraction- or repulsion-driven glassy behavior that are independent of the choice of reference length-scale. Specifically, we will study the difference between the MCT results computed with the full  $V(r)$  and those using the purely repulsive  $V_{\text{cut}}$  employed in the definition of the WCA- $\sigma_{\text{eff}}$ . The exponent parameter  $\lambda$  (Eqn. 7) and the non-ergodicity parameter  $f^c(q) = \lim_{t \rightarrow \infty} \phi^c(q, t)$  (given by Eqn. 5) will also be calculated, predicting, respectively, the form of the relaxation of density fluctuations and the strength of the arrest.

The first of these calculations is aimed at distinguishing the influence of the attractive part of the Girifalco

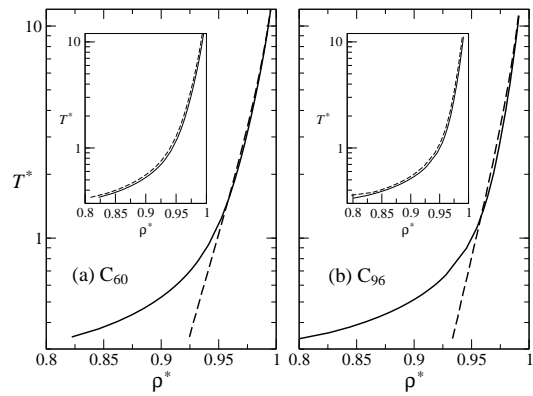


FIG. 3: Glass transition lines from MCT with the PY approximation for  $C_{60}$  (left panel) and  $C_{96}$  (right panel). The solid lines reproduce the transition lines from Fig. 2. The dashed lines correspond to the analogous results where the Girifalco potential has been replaced by its purely repulsive version,  $V_{\text{cut}}(r)$ , Eq. (4). Insets: solid lines are the full-potential transition lines, and dashed lines are those obtained from cutting off  $S(q)$  at low  $q$  in the MCT integral, see text for details.

potential on the glass transition from that of the repulsion. The MCT transition lines are computed for the cut-off Girifalco potential, Eq. (4), which excludes any attraction but retains the functional shape of the repulsive core. A similar comparison of the LJ model with its cut-off variant yields MCT transitions that are almost indistinguishable from each other [29], indicating that purely attractive effects are negligible for all temperatures.

As shown in Fig. 3 for  $C_{60}$  and  $C_{96}$ , the situation is different in the Girifalco potential. The glass transition obtained from the repulsive core of the potential only (dashed lines) only follows the full-potential result at very high temperatures. It shows a small deviation in the intermediate-temperature region, and below  $T^* \approx 1$  it deviates significantly: it bends over to much lower densities, indicating that for  $T^* \lesssim 1$ , attraction does matter for the glass transition.

This bend is a genuine kinetic, attraction-driven effect, and in particular not associated with the proximity of the spinodal. To confirm this, we plot (insets of Fig. 3) a comparison of the full-potential transition line with one obtained from a model that does have attraction, but no spinodal effects entering into MCT: the dashed lines in the insets of Fig. 3 were obtained by cutting off the  $S(q)$  determined from the full Girifalco potential at  $q < q_{\text{peak}}/3$ , thereby eliminating the sharp increase in  $S(q \rightarrow 0)$  signalling the approach to the spinodal. The resulting MCT transition is close to the one including the spinodal, indicating that the latter plays no important role, and in particular cannot be responsible for the discussed deviation of the attractive system from the purely repulsive one. Note that the small shift visible in the insets of the figure is due to the details of our cutoff procedure which overestimates the MCT coupling constants.

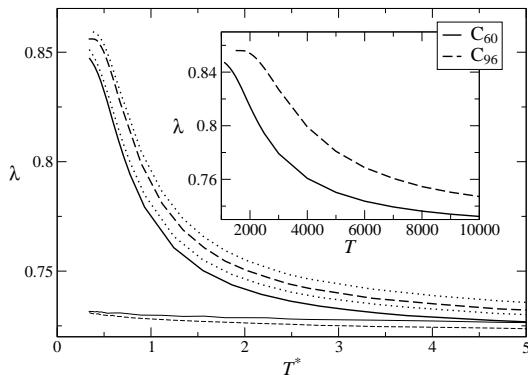


FIG. 4: MCT exponent parameter  $\lambda$  evaluated along the glass transition line, for  $C_{60}$  (solid lines) and  $C_{96}$  (dashed), as function of reduced temperature  $T^*$ . The upper set of curves corresponds to the full potential, while the lower corresponds to the cutoff potential, Eq. (4). Dotted lines are results evaluated from the full potential without the spinodal low- $q$  region. Inset:  $\lambda(T)$  plotted as a function of unscaled temperature.

Based on the above results we can conjecture that the Girifalco-model glass transition in the experimentally accessible temperature range shows strong attraction-induced effects. There exists a region at relatively low densities,  $0.8 < \rho^* \lesssim 0.95$ , where the Girifalco model displays a glassy region that would not be there for a purely repulsive mechanism. We note further that, also in Fig. 3, a “relative reentry” can be seen - there is a region  $1 < T^* < 10$  where the purely repulsive system classifies as *lower* densities than the one including attraction. Again, one can allude to the SWS here, where this phenomenon is observed for  $\delta \lesssim 0.1\sigma$ , albeit the reentry there is with respect to the hard-sphere transition value. In our case, the reentry is only relative to the repulsive-transition line; that the latter is not at constant  $\rho^*$  indicates that the Barker-Henderson effective diameter does not account completely for all soft-core effects.

If there is indeed a cross-over from a repulsive glass (at extremely high  $T$ ) to an attraction-affected one, the MCT exponent parameter  $\lambda$  should, according to the square-well analogy, show a corresponding change as a function of  $T^*$ , indicating the cross-over region by a peak. In Fig. 4, we plot the  $T^*$ -dependence of  $\lambda$  for the  $C_{60}$  and  $C_{96}$  potentials. Indeed,  $\lambda(T^*)$  rises significantly for  $T^* \lesssim 1$  and displays a peak at  $T^* \approx 0.5$  in both models. This peak is, however, quite close to the region where the glass transition line terminates at the spinodal, although it is in no way connected to it. The last statement is again seen from the  $\lambda(T^*)$  corresponding to the model with a low- $q$  cutoff in  $S(q)$  (see discussion of Fig. 3) being close to the full- $S(q)$  calculated one (the small rise in  $\lambda$  being due to the overestimation of the MCT coupling constants referred to earlier). In contrast, the purely repulsive systems according to Eq. (4) display a value  $\lambda \approx 0.73$  that is essentially independent of  $T^*$  and consistent with the values one gets for the Lennard-Jones or hard-sphere systems. Again, this clearly demonstrates the influence of

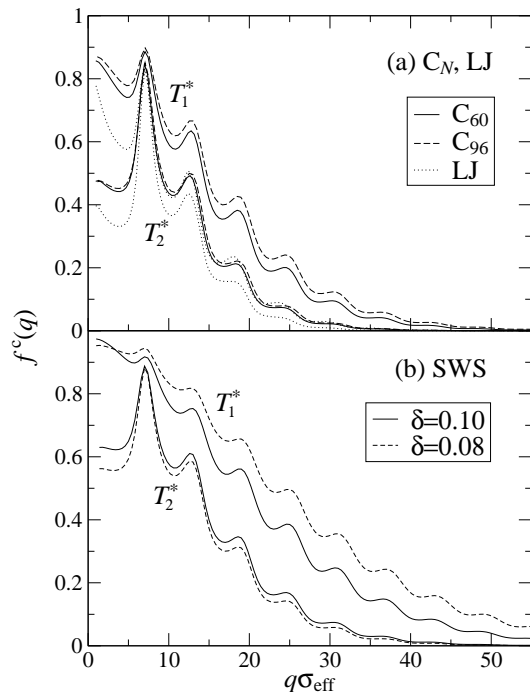


FIG. 5: Nonergodicity parameters  $f^c(q)$  at the MCT transition as functions of rescaled wave vector,  $q^* = q\sigma_{\text{eff}}^3$ . Upper panel:  $C_{60}$  (solid lines) and  $C_{96}$  (dashed); upper curves correspond to  $T_1^* = 0.5$ , lower curves to  $T_2^* = 2$  (PY approximation). The dotted lines show the corresponding results for the Lennard-Jones system. Lower panel:  $f^c(q)$  for the square-well system, with attraction range  $\delta = 0.10$  (solid lines) and  $\delta = 0.08$  (dashed), at temperatures  $T_1^* \approx 0.22$  and  $T_2^* = 0.5$  (MSA approximation).

attraction at sufficiently low temperatures.  $\lambda$  however remains bounded by 0.85 (0.86) for  $C_{60}$  ( $C_{96}$ ), hence no higher-order glass-transition singularity is predicted for these models. The peak in  $\lambda(T^*)$  increases somewhat with increasing  $N$ , i.e., with decreasing attraction range, so that one can conjecture the existence of a higher-order singularity in giant fullerene systems. But unrealistically large  $N$  would need to be considered for this.

As explained in Sec. III,  $\lambda$  determines the exponents for the asymptotic description of the time-dependent relaxation functions. To the “standard” value  $\lambda = 0.73$  correspond exponents  $a = 0.591$  and  $b = 0.314$ . In the  $C_{60}$  model, the values drop to  $a \approx 0.396$  and  $b \approx 0.250$  at the maximum in  $\lambda$ ; for  $C_{96}$  we similarly get  $a \approx 0.381$  and  $b \approx 0.244$ . However, these figures are still significantly different from zero, so that logarithmic decay is probably not observable in fullerene glass formers.

As mentioned above, attractive and repulsive glasses can be distinguished by their localization length, and similarly by the shape of the  $f^c(q)$  quantifying the degree of arrest. Figure 5 shows these plotted as functions of rescaled wave vector,  $q^* = q\sigma_{\text{eff}}^3$ , for  $T^* = 0.5$  (roughly corresponding to  $T \approx 1500$  K) and  $T^* = 2$ . A comparison with the corresponding LJ result (shown as dotted

lines) reveals that the Girifalco model predicts a higher degree of arrest than that occurring in the Lennard-Jones liquid: the  $f^c(q^*)$ -versus- $q^*$  curves for  $C_N$  are systematically above the LJ ones. In particular, there are two noteworthy trends exhibited by these curves, one upon changing temperature, the other upon changing  $N$ .

For the LJ system,  $f^c(q^*)$  changes relatively little with  $T^*$ , except for the low- $q$  region as the spinodal is approached. This increase in the  $q \rightarrow 0$  value is connected with the divergence of compressibility there. For the Girifalco models,  $f^c(q^*)$  changes rather more with temperature. Again, the fact that attraction plays an important role in the formation of fullerene glasses whereas it does not in LJ glasses, manifests itself here.

Shortening the attraction range with increasing  $N$ , we find the  $f^c(q^*)$  to increase at fixed  $T^*$ , indicating that particle caging is enhanced. Extracting a measure of the localization length from these curves, one concludes that this length shrinks with shrinking width of attraction. However, from the half-width of the  $f^c(q^*)$ -versus- $q^*$  curve one still estimates localization lengths of the order of 5% for the systems studied here, rendering them intermediate between the LJ reference system and the truly short-ranged SWS. To highlight the connection to this SWS, we show in the lower panel of Fig. 5 similar  $f^c(q^*)$  for two such systems,  $\delta = 0.1$  and  $\delta = 0.08$ . This leads to localization lengths that are approximately those observed in the Girifalco system. Also, the values of  $\lambda$  are similar:  $\lambda \approx 0.81$  for  $\delta = 0.08$  and  $\lambda \approx 0.79$  for  $\delta = 0.10$  at  $T_1^*$ , to be compared with  $\lambda \approx 0.83$  for  $C_{60}$  (see Fig. 4).

Again, as  $T^*$  is lowered, a cross-over occurs from relatively narrow  $f^c(q^*)$ -versus- $q^*$  curves to significantly wider ones, signalling the crossover from a repulsive to an attraction-driven glass. Note that the numerical values for  $T_1^* < T_2^*$  cannot be compared immediately, since the SWS data has been obtained in the mean-spherical approximation (MSA) to  $S(q)$ , which results in an intrinsically different  $T^*$ -scale [27]. In the SWS data shown, the crossover is more evident than it is in the Girifalco model. Note that neither of the two SWS are short-ranged enough to exhibit a higher-order glass transition.

The comparison with the SWS leads quite naturally to the question how to define an effective attraction range  $\delta_{\text{eff}}$  for smooth potentials such as the Girifalco one. One such definition has been proposed by Noro and Frenkel [54] and is based on an extended law of corresponding states: one compares systems with smooth interactions to a SWS at a corresponding state (in terms of rescaled density and temperature), for which also the second virial coefficient relative to that of a HS system,  $B_2^*$ , is matched. Since  $B_2^*$  depends on the attraction range, this gives a prescription to determine an  $\delta_{\text{eff}}$ . From the Noro/Frenkel mapping we read off  $\delta_{\text{eff}} \approx 0.14$  for the  $T^* \approx 0.5$  discussed in Fig. 5. However, it appears that the values of  $\lambda$  correspond more closely to a SWS with a narrower range,  $\delta \lesssim 0.10$ . This can be rationalized easily: the mapping by Noro and Frenkel emphasizes a correspondence of  $B_2^*$ , which is argued to take on roughly constant values close

to the liquid-gas critical point. The physical mechanisms responsible for the change in  $f^c(q)$ , on the other hand, are quite different from the spinodal effects, as pointed out in connection with Figs. 2 and 3. There is no reason to expect that a  $\delta_{\text{eff}}$  suitable for mapping the spinodal region will be the most useful one to map the glass-transition region to that of a SWS.

## V. CONCLUSIONS

We have calculated idealized glass transition lines for a number of fullerene systems with various sizes, using the mode-coupling theory of the glass transition and an effective pair-potential description. Our results are readily testable using molecular-dynamics computer simulation, such as performed recently [30, 31, 32].

Glass transition lines are found for densities of the order of  $1 \text{ nm}^{-3}$  for  $C_{60}$ , bending over to slightly lower densities at temperatures below the gas-liquid critical point. The results for  $C_{70}$  and  $C_{96}$  are qualitatively similar, but shifted in the temperature-density plane according to the change in natural energy and length scales of the different systems. At least within MCT, these glass transitions, being purely kinetic in origin, appear completely unrelated to the gas-liquid spinodal or similar thermodynamic questions, and hence to the long-standing question whether fullerene liquids are stable or only metastable with respect to sublimation. Note also that a common way to suppress crystallization and hence study the metastable liquid in colloidal suspensions is to make use of their polydispersity. It might be interesting whether a similar polydispersity arising in the production of fullerenes [55] could play the equivalent role, something that has already been indicated in simulation studies of binary fullerene mixtures [32]. Finally, in the observation of our predicted MCT transition line, one will need to consider (in analogy to standard molecular liquids) the problem of additional (hopping) relaxation processes, which may cutoff the MCT transition as such, to different extent at different temperatures. However, the observability of our predictions should be not worse than in other molecular liquids, where MCT has been applied with great success at least in a limited region on the liquid-side of the transition [48].

The glass transitions we have discussed are strongly influenced by inter-particle attraction, which is, at least within MCT, a clear contrast to standard molecular glasses where interactions are well described by Lennard-Jones type potentials. This attraction-domination leads to an occurrence of the glass transition at lower densities than in the purely repulsive system. It manifests itself in several ways, in particular through MCT's exponent parameter  $\lambda$  and the plateau values of the time-dependent correlation functions (or the glass form factors). The exponent parameter,  $\lambda \gtrsim 0.85$  at typical temperatures, is found to be significantly higher than in LJ glasses ( $\lambda \approx 0.73$ ), leading to lower exponents  $a$  and  $b$  for the

asymptotic description of the time-dependent relaxation in terms of power laws. It should be possible to observe this difference, for example by an asymptotic analysis of correlation functions measured in MD simulations [48]. Also, the asymptotic form of the divergence of relaxation times or the diffusivity close to  $T_c$  is governed by these exponents,  $\tau \sim |T - T_c|^{-\gamma}$  with  $\gamma = 1/(2a) + 1/(2b)$ . Note that  $\gamma \approx 2.44$  in the hard-sphere system, while our calculations predict  $\gamma \approx 3.46$  for the attraction-affected part of the fullerene glass transition. The final decay of the correlation function is also often fitted with a stretched exponential law,  $\phi(q, t) \approx A(q) \exp[-(t/\tau(q))^\beta]$ , with some  $A(q) \leq f^c(q)$  and a stretching exponent  $\beta(q) < 1$ . For  $q \rightarrow \infty$ ,  $\beta(q) \rightarrow b$  [56]; thus  $b$  can be taken as a measure of the ‘stretching’ exhibited by the correlation functions: low values of  $b$  will correspond to a more stretched decay. It is conceivable that such an analysis of dynamical correlation functions will reveal a much broader relaxation spectrum than in usual glasses. Such tests have, to our knowledge, not been performed yet.

As a second signature, the glass form factors  $f^c(q)$  within the Girifalco model are noticeably higher than for corresponding LJ states: the fullerene glass is predicted to be relatively stiff, featuring relatively high plateaus in the dynamical two-step relaxation process over a wider wave-vector range than usually observed in molecular glasses: in the LJ system, this plateau has basically dropped to zero for  $q\sigma_{\text{eff}} \approx 30$ , while we calculate  $f^c > 0.1$  still at this wave vector for the Girifalco system. There, one needs to reach wave vectors  $q\sigma_{\text{eff}} \approx 50$  before the amplitude of the final relaxation process vanishes. From the trend observed in  $f^c(q)$ , we argue that for  $C_N$  glasses, the localization length (a measure of the average cage size) should scale with  $1/N$ , i.e., with the inverse size of the fullerene molecule and therefore its relative attraction range. This scaling is similar to that observed in attraction-driven square-well systems, and opposite to that in the standard class of repulsive systems. Comparison of our predictions for  $f^c(q)$  with simulations or experiment would require a rescaling of density [57] and probably also temperature [58] as a result of the tendency of MCT to underestimate the coupling required to produce arrest [58, 59]. It is possible that the conclusion of Abramo *et al* [30, 31] that the glass transition in  $C_{60}$  is hard-sphere-like (from the collapse of their data to a vertical line using the WCA- $\sigma_{\text{eff}}$ ) is a result of the fact that the molecular dynamics transition is shifted to lower tem-

peratures (higher couplings) than that in MCT. Lower temperatures and densities (if accessible) might then be required to see the effects of attraction.

Note that  $f^c(q)$  is usually predicted from MCT with much better accuracy than e.g.  $T_c$ , leading to often quantitatively correct results. Measurements of  $f^c(q)$  would therefore be highly desirable, allowing both a test of MCT and an estimate of its error in terms of density and temperature.

Attraction-dominated in the sense discussed above, however, does not imply the phenomena of *very short-ranged* strong attraction, as they have been discussed in the field of colloid-polymer mixtures. Their hallmarks are logarithmic decays in the time-dependent relaxation; in this respect, the fullerene systems we have studied are only intermediate in terms of their attraction range. However, attempting to map the results to those obtained for square-well systems can still prove useful, as our comparison of  $f^c(q)$  results indicates.

In particular, they can be used to define an effective attraction range of the fullerene (or similar) systems. We want to emphasize that such a definition is not unique, and might well depend on the physical problem one is interested in. Previous discussions have argued mainly in terms of a nearly vanishing stable-liquid pocket, emphasizing the metastability of the liquid-gas spinodal as a signature of short-ranged attractions. If one, however, is interested in high-density kinetic phenomena, the underlying physical mechanisms mediated by the attraction have little in common with those in the vicinity of the spinodal, and hence a different measure of effective attraction range needs to be used. Such a measure could be based on demanding equality between the  $f^c(q)$ , or, less stringently, the localization length at the glass transition. If one is concerned with glassy dynamics, the best measure might be to introduce a ‘‘law of corresponding glasses’’ based on the MCT exponent parameter, demanding  $\lambda(T^*) = \lambda_{\text{SWS}}(T^*, \delta_{\text{eff}}(T^*))$  to determine  $\delta_{\text{eff}}$ .

## Acknowledgments

We thank M.E. Cates for valuable comments. This research was funded by EPSRC grant GR/S10377. Th.V. acknowledges financial support through DFG grant Vo 1270/1-1.

- 
- [1] H. W. Kroto, J. R. Heath, S. C. O’Brien, R. F. Curl, and R. E. Smalley, *Nature (London)* **318**, 162 (1985).
  - [2] W. Krätschmer, L. D. Lamb, K. Fostiropoulos, and D. R. Huffman, *Nature (London)* **347**, 354 (1990).
  - [3] C. Z. Wang, C. H. Xu, C. T. Chan, and K. M. Ho, *J. Phys. Chem.* **96**, 3563 (1992).
  - [4] C. Xu and G. E. Scuseria, *Phys. Rev. Lett.* **72**, 669 (1994).
  - [5] S. G. Kim and D. Tománek, *Phys. Rev. Lett.* **72**, 2418 (1994).
  - [6] K. Ohno, Y. Maruyama, and Y. Kawazoe, *Phys. Rev. B* **53**, 4078 (1996).
  - [7] S. Serra, S. Sanguinetti, and L. Colombo, *Chem. Phys. Lett.* **225**, 191 (1994).
  - [8] M. R. Stetzer, P. A. Heiney, J. E. Fischer, and A. R. McGhie, *Phys. Rev. B* **55**, 127 (1997).

- [9] C. S. Sundar, A. Bharathi, Y. Hariharan, J. Janaki, V. Sankara Sastry, and T. S. Radhakrishnan, *Solid State Commun.* **84**, 823 (1992).
- [10] S. D. Leifer, D. G. Goodwin, M. S. Anderson, and J. R. Anderson, *Phys. Rev. B* **51**, 9973 (1995).
- [11] M. Moseler, H. Riedel, P. Gumbusch, J. Ståring, and B. Mehlig, *Phys. Rev. Lett.* **94**, 165503 (2005).
- [12] M. C. Abramo and C. Caccamo, *J. Chem. Phys.* **106**, 6475 (1997).
- [13] A. Cheng, M. L. Klein, and C. Caccamo, *Phys. Rev. Lett.* **71**, 1200 (1993).
- [14] M. H. J. Hagen, E. J. Meijer, G. C. A. M. Mooij, D. Frenkel, and H. N. W. Lekkerkerker, *Nature (London)* **365**, 425 (1993).
- [15] N. W. Ashcroft, *Nature (London)* **365**, 387 (1993).
- [16] L. Mederos and G. Navascués, *Phys. Rev. B* **50**, 1301 (1994).
- [17] F. M. S. Silva Fernandes, F. F. M. Freitas, and R. P. S. Fartaria, *J. Phys. Chem. B* **107**, 276 (2003).
- [18] B. Chen, J. I. Siepmann, S. Karaborni, and M. L. Klein, *J. Phys. Chem. B* **107**, 12320 (2003).
- [19] P. Bolhuis, M. Hagen, and D. Frenkel, *Phys. Rev. E* **50**, 4880 (1994).
- [20] C. Rascón, G. Navascués, and L. Mederos, *Phys. Rev. B* **51**, 14899 (1995).
- [21] A. P. Gast, C. K. Hall, and W. B. Russel, *J. Colloid Interface Sci.* **251**, 251 (1983).
- [22] H. N. W. Lekkerkerker, W. C. K. Poon, P. N. Pusey, A. Stroobants, and P. B. Warren, *Europhys. Lett.* **20**, 559 (1992).
- [23] C. S. Yannoni, R. D. Johnson, G. Meijer, D. S. Bethune, and J. R. Salem, *J. Phys. Chem.* **95**, 9 (1991).
- [24] K. N. Pham, A. M. Puertas, J. Bergenholtz, S. U. Egelhaaf, A. Moussaïd, P. N. Pusey, A. B. Schofield, M. E. Cates, M. Fuchs, and W. C. K. Poon, *Science* **296**, 104 (2002).
- [25] T. Eckert and E. Bartsch, *Phys. Rev. Lett.* **89**, 125701 (2002).
- [26] J. Bergenholtz and M. Fuchs, *Phys. Rev. E* **59**, 5706 (1999).
- [27] K. Dawson, G. Foffi, M. Fuchs, W. Götze, F. Sciortino, M. Sperl, P. Tartaglia, and Th. Voigtmann, *Phys. Rev. E* **63**, 011401 (2001).
- [28] B. Widom, *Science* **157**, 375 (1967).
- [29] Th. Voigtmann (2006), in preparation.
- [30] M. C. Abramo, C. Caccamo, D. Rosta, and R. Ruberto, *J. Phys. Chem. B* **108**, 13576 (2004).
- [31] M. C. Abramo, C. Caccamo, D. Costa, and R. Ruberto, *J. Phys. Chem. B* **109**, 24077 (2005).
- [32] R. Ruberto, M. C. Abramo, and C. Caccamo, *Phys. Rev. B* **70**, 155413 (2004).
- [33] F. Gugenberger, R. Heid, C. Meingast, P. Adelman, M. Braun, H. Wühl, M. Haluska, and H. Kuzmany, *Phys. Rev. Lett.* **69**, 3774 (1992).
- [34] W. Götze, in *Liquids, Freezing and Glass Transition*, edited by J. P. Hansen, D. Levesque, and J. Zinn-Justin (North Holland, Amsterdam, 1991), Les Houches Summer Schools of Theoretical Physics Session LI (1989), pp. 287–503.
- [35] L. A. Girifalco, *J. Phys. Chem.* **95**, 5370 (1991).
- [36] K. Kniaź, L. A. Girifalco, and J. E. Fisher, *J. Phys. Chem.* **99**, 16804 (1995).
- [37] M. C. Abramo and C. Caccamo, *Phys. Chem. Solids* **57**, 1751 (1996).
- [38] B.-C. Wang, H.-W. Wang, J.-C. Chang, H.-C. Tso, and Y.-M. Chou, *J. Molec. Struct. (Theochem.)* **540**, 171 (2001).
- [39] V. I. Zubov, *Molec. Mater.* **13**, 385 (2000).
- [40] M. C. Abramo, C. Caccamo, D. Costa, and G. Pellicane, *Europhys. Lett.* **54**, 468 (2001).
- [41] J. M. Pacheco and J. P. Prates Ramalho, *Phys. Rev. Lett.* **79**, 3873 (1997).
- [42] J. A. Barker and D. Henderson, *J. Chem. Phys.* **47**, 4714 (1967).
- [43] J. D. Weeks, D. Chandler, and H. C. Andersen, *J. Chem. Phys.* **54**, 5237 (1971).
- [44] J.-P. Hansen and I. R. McDonald, *Theory of Simple Liquids* (Academic Press, London, 1986), 2nd ed.
- [45] C. Caccamo, *Phys. Rep.* **274**, 1 (1996).
- [46] S. Labik, A. Malijevsky, and P. Vonka, *Molec. Phys.* **56**, 709 (1985).
- [47] M. M. G. Alemany, C. Rey, O. Diéguez, and L. J. Gallego, *J. Chem. Phys.* **112**, 10711 (2000).
- [48] W. Götze, *J. Phys.: Condens. Matter* **11**, A1 (1999).
- [49] H. Z. Cummins, *J. Phys.: Condens. Matter* **11**, A95 (1999).
- [50] W. Götze and M. Sperl, *Phys. Rev. E* **66**, 011405 (2002).
- [51] A. M. Puertas, M. Fuchs, and M. E. Cates, *Phys. Rev. Lett.* **88**, 098301 (2002).
- [52] F. Sciortino, P. Tartaglia, and E. Zaccarelli, *Phys. Rev. Lett.* **91**, 268301 (2003).
- [53] T. Franosch, M. Fuchs, W. Götze, M. R. Mayr, and A. P. Singh, *Phys. Rev. E* **55**, 7153 (1997).
- [54] M. G. Noro and D. Frenkel, *J. Chem. Phys.* **113**, 2941 (2000).
- [55] J. Sloan, R. E. Dunin-Borkowski, J. L. Hutchison, K. S. Coleman, V. C. Williams, J. B. Claridge, A. P. E. York, C. Xu, S. R. Bailey, G. Brown, et al., *Chem. Phys. Lett.* **316**, 191 (2000).
- [56] M. Fuchs, *J. Non-Cryst. Solids* **172–174**, 241 (1994).
- [57] W. van Meegen and S. M. Underwood, *Phys. Rev. Lett.* **70**, 2766 (1993).
- [58] M. Sperl, *Phys. Rev. E* **69**, 011401 (2004).
- [59] J. Bergenholtz, W. C. K. Poon, and M. Fuchs, *Langmuir* **19**, 4493 (2003).